CrossMark

Switchbacks in the Near-Sun Magnetic Field: Long Memory and Impact on the Turbulence Cascade

Thierry Dudok de Wit[1], Vladimir V. Krasnoselskikh[1], Stuart D. Bale[2,3,4,5], John W. Bonnell[3], Trevor A. Bowen[3], Christopher H. K. Chen[5], Clara Froment[1], Keith Goetz[6], Peter R. Harvey[3], Vamsee Krishna Jagarlamudi[1], Andrea Larosa[1], Robert J. MacDowall[7], David M. Malaspina[8], William H. Matthaeus[9], Marc Pulupa[3], Marco Velli[10], and Phyllis L. Whittlesey[3]

[1] LPC2E, CNRS and University of Orléans, 3A avenue de la Recherche Scientifique, Orléans, France; ddwit@cnrs-orleans.fr
[2] Physics Department, University of California, Berkeley, CA 94720-7300, USA
[3] Space Sciences Laboratory, University of California, Berkeley, CA 94720-7450, USA
[4] The Blackett Laboratory, Imperial College London, London, SW7 2AZ, UK
[5] School of Physics and Astronomy, Queen Mary University of London, London E1 4NS, UK
[6] School of Physics and Astronomy, University of Minnesota, Minneapolis, MN 55455, USA
[7] Solar System Exploration Division, NASA/Goddard Space Flight Center, Greenbelt, MD 20771, USA
[8] Laboratory for Atmospheric and Space Physics, University of Colorado, Boulder, CO 80303, USA
[9] Department of Physics and Astronomy, University of Delaware, Newark, DE 19716, USA
[10] Institute of Geophysics & Planetary Physics, Department of Earth, Planetary & Space Sciences, University of California, Los Angeles, CA 90095-1567, USA

Abstract

One of the most striking observations made by *Parker Solar Probe* during its first solar encounter is the omnipresence of rapid polarity reversals in a magnetic field that is otherwise mostly radial. These so-called switchbacks strongly affect the dynamics of the magnetic field. We concentrate here on their macroscopic properties. First, we find that these structures are self-similar, and have neither a characteristic magnitude, nor a characteristic duration. Their waiting time statistics show evidence of aggregation. The associated long memory resides in their occurrence rate, and is not inherent to the background fluctuations. Interestingly, the spectral properties of inertial range turbulence differ inside and outside of switchback structures; in the latter the $1/f$ range extends to higher frequencies. These results suggest that outside of these structures we are in the presence of lower-amplitude fluctuations with a shorter turbulent inertial range. We conjecture that these correspond to a pristine solar wind.

1. Introduction

In November 2018 *Parker Solar Probe* (Fox et al. 2015) became the closest spacecraft to the Sun, reaching a distance of $35.7\,R_{\odot}$ or 0.166 au from our star. This was the first of a series of 26 encounters during which the spacecraft will perform in situ and remote sensing observations of the solar corona and gradually get as close as $9.8\,R_{\odot}$. This first encounter, however, has already provided a wealth of new results (Bale et al. 2019; Howard et al. 2019; Kasper et al. 2019; McComas et al. 2019). Among these is the omnipresence of swift reversals of the magnetic field, which is otherwise mostly radial. The elusive origin of these transient events, often called switchbacks, and their potential role in heating the solar wind, has spurred active discussions. A global understanding of these switchbacks is gradually emerging as detailed comparisons of the different observations progress. Here, we consider these events from a more macroscopic point of view, and investigate what new insights can be gained from the dynamics of the magnetic field.

The solar wind is a fascinating laboratory for studying waves and turbulence in collisionless plasmas (Bruno & Carbone 2013). However, by the time the wind that emanates from the Sun has reached the Earth's orbit (where most in situ measurements are performed) it has already evolved dynamically for several days such that the properties of the pristine wind that *Parker Solar Probe* aims at observing are blurred. During its first perihelion pass, the spacecraft was almost corotating with the Sun and

mostly observed a slow solar wind emerging from a small coronal hole located near the equator (Bale et al. 2019; Badman et al. 2020). For more than 10 days around the first perihelion, the magnetic field was essentially radial with clear sunward polarity. This regularity was continuously interrupted by switchbacks; see Figure 1.

Switchbacks are characterized by their high Alfvénicity, the absence of notable temperature changes, and an increase in the wind velocity by approximately 20% (Bale et al. 2019; Kasper et al. 2019). Likewise, the proton density also tends to increase inside these switchbacks. The Alfvénicicity is attested by the low relative variability of the total magnetic field. The duration of these switchbacks ranges from less than a second to more than one hour. A remarkable result is the occasional presence of periods of quiet solar wind with low levels of magnetic field fluctuations and coherent wave activity (Bowen et al. 2020; Malaspina et al. 2020).

Sudden reversals of the magnetic field have been observed for several decades. Early examples can be spotted in observations from the *Helios* mission (Behannon & Burlaga 1981). These reversals have since been studied at various distances from the Sun (Kahler et al. 1996; van Ballegooijen et al. 1998; Balogh et al. 1999; Yamauchi et al. 2004; Landi et al. 2006; Neugebauer 2012; Neugebauer & Goldstein 2013; Matteini et al. 2014; Borovsky 2016; Horbury et al. 2018), and in simulations (Velli et al. 2011). However, the observations made by *Parker Solar Probe* stand out because: (1) the absence of major velocity
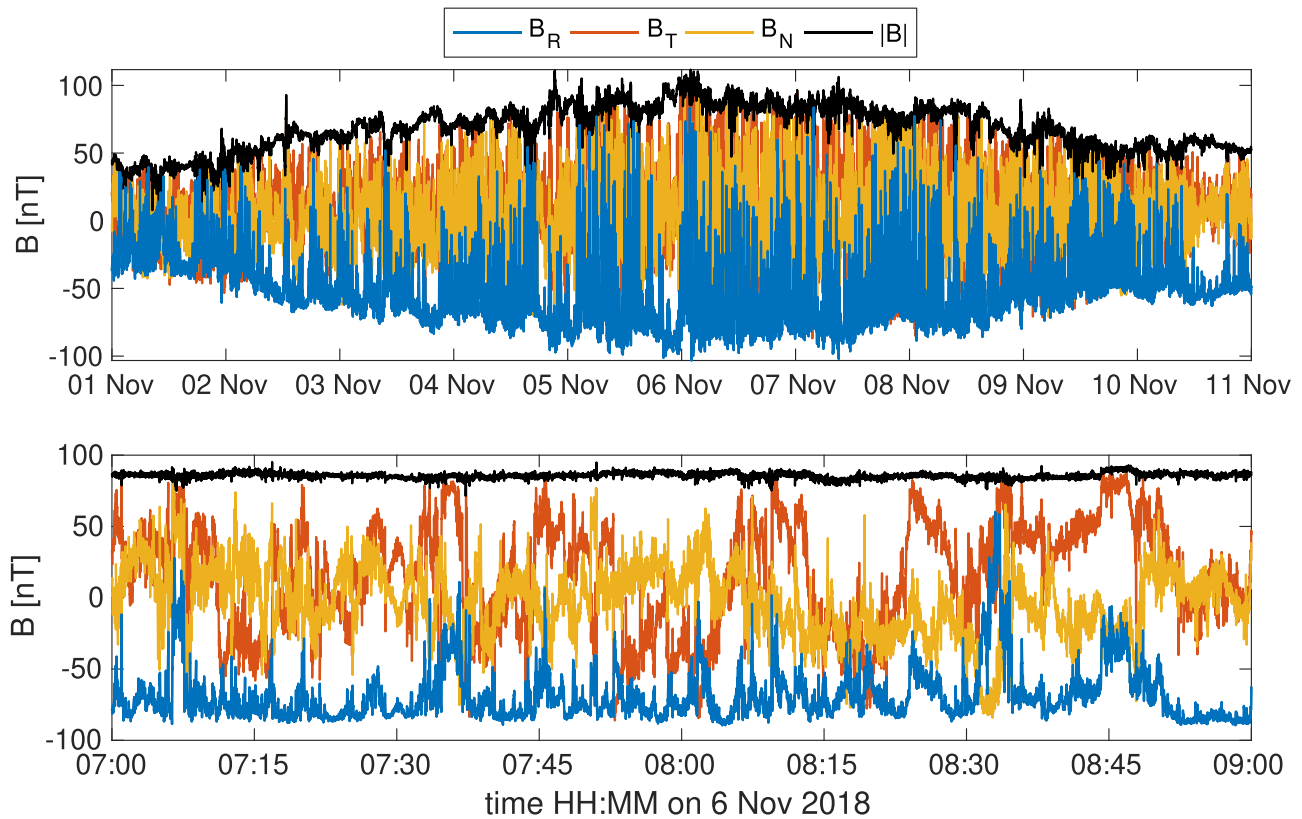
Figure 1. Magnetic field for the whole interval of interest (top plot) and for a 2 hr excerpt (bottom plot). An RTN coordinate system is used; see Section 2.

increase during switchbacks as compared to what has been observed, for example, by *Helios* at 0.3 au (Borovsky 2016); (2) their observation in a slow (but Alfvénic) stream; and (3) the sharpness and omnipresence of these events, as if the coronal plasma was continuously transitioning between two metastable states: one in which the magnetic field is pointing sunward along the Parker spiral, and one in which it is deflected away from the spiral, sometimes by as much as 180°.

Several (and mutually not exclusive) explanations have been proposed for these switchbacks, such as plasma jets associated with reconnection events deep inside the corona, or the crossing of kinked magnetic flux tubes, of closed magnetic loops, or of large-amplitude, non-compressive Alfvén waves similar to those observed by Belcher & Davis (1971). The properties of the monodirectional energetic electron beams (Whittlesey et al. 2019) and the inversion of the magnetic helicity (McManus et al. 2020) inside of the switchbacks give support to the idea that these structures are localized twists in the magnetic field and not polarity reversals or closed loops.

A consequence of the elusive origin of these switchbacks is the lack of consensus on their terminology. These structures are also called foldings, (intrasector) field reversals, jets, spikes, or deflections. They are truly deflections but we shall refer to them as switchbacks.

Interestingly, the presence of abrupt flow reversals is not unique to plasmas and has also been observed in hydrodynamic turbulence at high Rayleigh numbers (Araujo et al. 2005) and in the geomagnetic field (Sorriso-Valvo et al. 2007). There are also analogies with dynamical systems that exhibit transitions between different states (Nicolis 1993; Benzi 2005). Metastable systems that are in contact with a (possibly external) perturbation have received considerable attention in the framework of

non-equilibrium physics because they are capable of exhibiting effects that cannot be observed when the system is in thermal equilibrium (Gammaitoni et al. 1998). One of these effects is fluctuation amplification through stochastic resonance.

All these systems raise the same question: how can such transitions occur when their lifetime is so much longer than the characteristic timescales of the system? In the context of the solar wind, a related question is: are these deflections part of the turbulent wave field or are they signatures of perturbations that are generated by some external mechanism such as the moving photospheric footpoint of magnetic flux tubes? Beforehand, we should define what a switchback is. To answer these questions, we investigate here the dynamical properties of the magnetic field, following an exploratory approach.

This macroscopic exploration of the solar magnetic field is organized as follows: after presenting the data in Section 2 we address their main properties in Section 3, followed by their waiting time statistics in Section 4, and a focus on signatures of long memory in Section 5. Finally, we discuss the implications of our perception of solar wind turbulence in Section 6 and conclude in Section 7.

2. Data

The vector magnetic field is measured on board *Parker Solar Probe* by the MAG magnetometer from the FIELDS consortium (Bale et al. 2016). At perihelion, the cadence of MAG goes up to 292.97 samples per second. Since we are interested in much lower frequencies, in what follows all observations will be decimated to 73.24 Hz.

Our time interval of interest is centered on the first perihelion pass of 2018 November 6, and runs from November 1st to 2018 November 10. During that 10 day interval the spacecraft
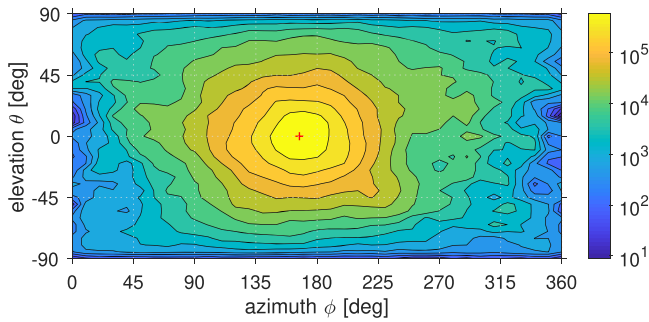
Figure 2. 2D histogram of the angular deflection of the magnetic field, for the full time interval. The orientation of the Parker spiral for prevailing solar wind conditions during the encounter is indicated by a cross. An azimuth of 180° corresponds to a sunward pointing of the magnetic field.

was almost corotating with the Sun, such that temporal variations are primarily associated with spatial structures that are advected past the spacecraft with a typical solar wind speed of 220 km s^{-1}–450 km s^{-1} (Kasper et al. 2019). This means that the crossing of thin structures such as filaments may take considerably longer than what other spacecraft usually see in the solar wind.

During that whole interval the photospheric footpoint of *Parker Solar Probe* was mostly located in the same equatorial coronal hole (Badman et al. 2020), causing the spacecraft to be immersed in a relative stable and highly Alfvénic slow solar wind. Outside of the interval the conditions progressively started changing with, for example, the occurrence of heliospheric perturbations, such as a flux rope on November 12. The distance to the Sun varied from 51.4 to 35.7 $R_\odot$ and the median deviation of the magnetic field from the radial direction was 12°.4.

In the following we express the magnetic field in the RTN coordinate system: R is radial and points away from the Sun, the tangential T component is the cross-product of the solar rotation vector with R; and the normal N component completes the right-handed set and points in the same direction as the solar rotation vector.

3. Macroscopic Properties of the Switchbacks

Figure 1 illustrates the main properties of the magnetic field, with conspicuous reversals in the radial B_R component that are the hallmark of switchbacks. These deflections come in all magnitudes: some cover a few degrees only, whereas the largest ones are fully anti-sunward. The high Alfvénicity is attested by the nearly constant total magnetic field.

Let us first determine whether these deflections have a preferred angular orientation. Figure 2 shows an occurrence histogram versus the azimuth and elevation of all the 67′108′864 observations of the magnetic field that were recorded during the 10 day interval. What stands out is the isotropic distribution of the deflections, with a strong concentration around an azimuth of 170°; the latter coincides with the average position of the Parker spiral, which is indicated by a cross on the plot. We conclude that the bulk of the deflections has an isotropic distribution around the direction of the Parker spiral.

Figure 2 shows that large deflections are more sporadic than small ones. The largest ones also have a preferential tangential orientation (Kasper et al. 2019; Horbury et al. 2020). In what follows we shall concentrate on the salient features of the deflections and therefore ignore the weak anisotropy that

affects the few largest events. Let us stress that this 2D distribution of the deflections does not significantly change when we estimate it separately for each of the 10 days of the interval of interest.

Thanks to the isotropy of the distribution of deflections we can now describe the dynamics of the magnetic field by means of one single parameter, which is its angular deflection with respect to the Parker spiral or mean magnetic field $\langle \boldsymbol{B} \rangle$. By analogy with magnetic lattices such as the Ising model (Peierls 1936), let us consider the potential energy associated with each deflection

$$E_p = -\boldsymbol{B} \cdot \langle \boldsymbol{B} \rangle, \quad (1)$$

where $\langle \boldsymbol{B} \rangle$ is the prevalent magnetic field. Because of the high Alfvénicity, the magnitude of the magnetic field may be considered as being close to constant, mainly varying with the distance from the Sun. Therefore, the potential energy is mainly proportional to $-\cos\alpha$, where α is the angle of deflection. Based on this we introduce the dimensionless *normalized deflection* $0 \leqslant z \leqslant 1$ as

$$z = \frac{1}{2}(1 - \cos\alpha), \quad (2)$$

as a convenient proxy for the deflection. Values that are close to 0 correspond to a "ground state" with a magnetic field that is aligned along the Parker spiral and pointing sunward. Gosling et al. (2009) had already noted that Alfvénic perturbations in the solar wind should be considered as deviations relative to a base value rather than to a time average. Conversely, z reaches 1 when the magnetic field is pointing anti-sunward and along the Parker spiral. With this definition we can now decouple geometrical variations from weak but still omnipresent amplitude changes in the magnetic field.

Figure 3 illustrates the difference between the radial magnetic field and the normalized deflection. Later in this study we shall discriminate deflections based on their value of z.

Note that the prevalent orientation of the mean magnetic field fluctuates in time regardless of the presence of switchbacks. There are multiple reasons for this, including changes in the velocity of the solar wind, and of the distance from the Sun. We find that 95% of the azimuthal orientations of the prevalent magnetic field (estimated from a running median over 6 hr intervals) are comprised between −5°.5 and 19°.1. Likewise, 95% of the elevations are between −10°.6 and 10°.6. These fluctuations cannot be neglected, as they affect the value of the normalized deflection; see Equation (1). Therefore, all deflections will be determined with respect to the direction of the prevalent magnetic field, as estimated from a running median over 6 hr intervals. Taking longer intervals does not affect the conclusions of our study. Shorter intervals are not allowed, since they must exceed the duration of the longest switchbacks. The jitter that results in the orientation of the prevalent field prevents us from distinguishing small variations in z. Therefore, in what follows, we shall systematically consider $z = 0.05$ as the threshold value below which the magnetic field is in a so-called ground state with small deflections.

The question now arises whether the distribution of z shows any evidence for thresholds that would allow us to define what a switchback is. This would not only help clarify the terminology but also give deeper insights into the physics. A
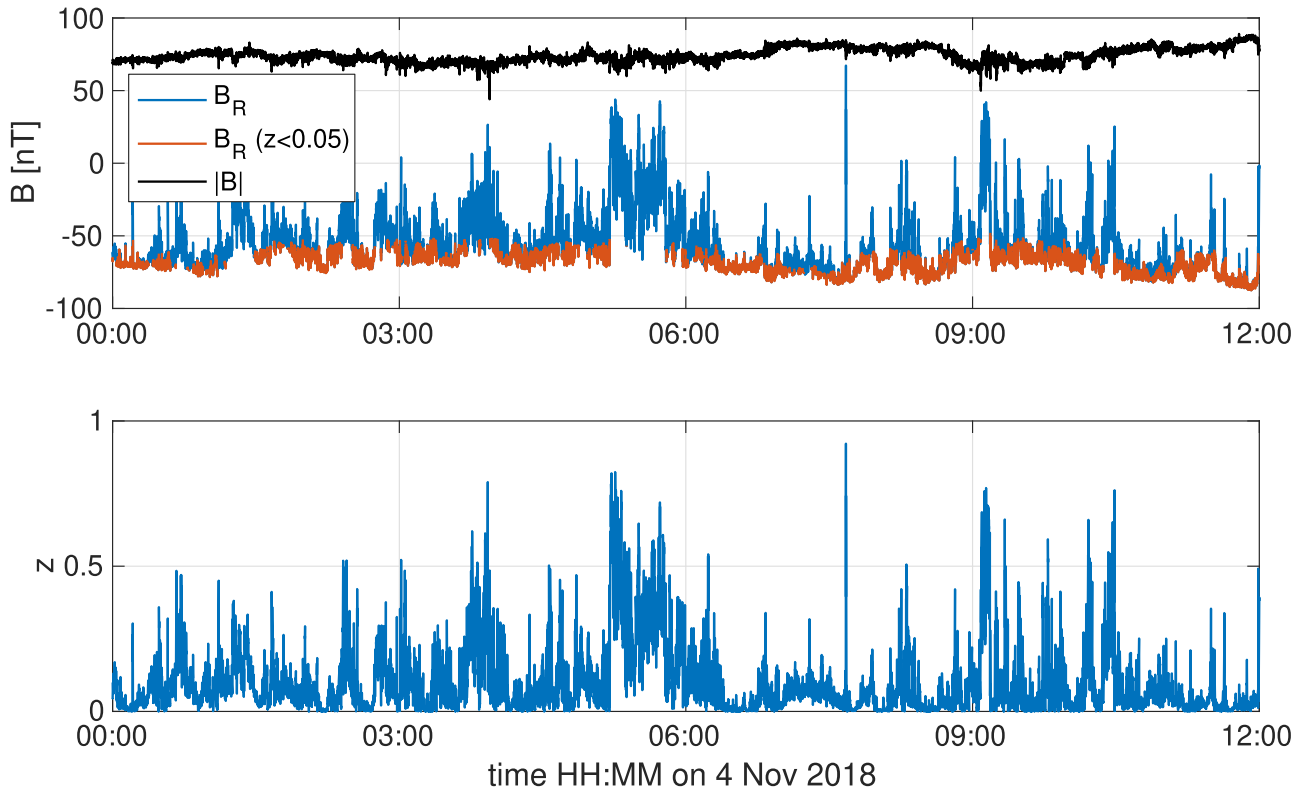
Figure 3. Excerpt of the radial component of the magnetic field and the total magnetic field (top plot) and the corresponding values of the normalized deflection z (bottom plot). Values of B_R that correspond to a small normalized deflection of $z < 0.05$ are highlighted.

bimodal distribution of z, for example, would indicate that the magnetic field oscillates between two metastable states.

The distribution of z is shown in Figure 4, which reveals a monotonic and rather featureless distribution apart from a small excess of small deflections. We are therefore in the presence of a continuum of self-affine deflections with no particular threshold that would allow us to define quantitatively what a switchback is. We would have reached the same conclusions using the deflection angle α.

We made various attempts to identify switchbacks by other means, such as their spectral signature. Farge & Schneider (2015) have shown how coherent structures such as vortices can be separated from background fluctuations by means of the wavelet transform. We were unable to achieve a comparable separation between large switchbacks and the less deflected magnetic field, presumably because the spectral content does not provide enough leverage for disentangling the two.

Note that the distribution shown in Figure 4 corresponds to deflections of all values of the magnetic field and not individual switchback events. For the latter we need a definition of what a switchback is. At the coarsest level one could define it as a deflection that exceeds the threshold value of $z = 0.05$, and then drops again below it. With this definition we can investigate the distribution of the peak deflection per switchback. This distribution (not shown) is steeper than that of Figure 4. However, it is equally devoid of discontinuities and therefore corroborates the idea that there is no typical deflection for defining a switchback.

4. Waiting Time Statistics

A key question is whether consecutive switchbacks tend to aggregate or are independent. For this we consider the statistical
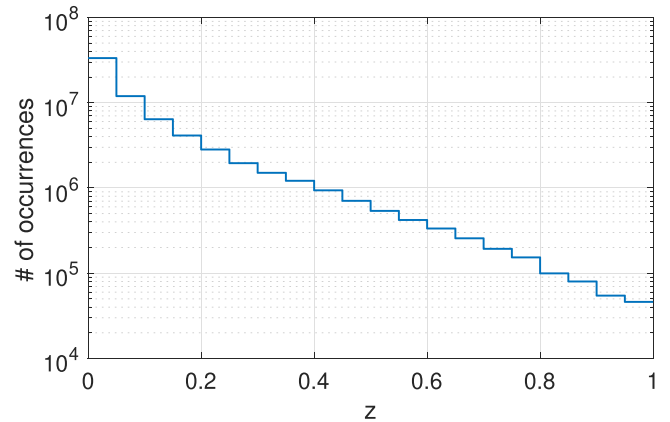
Figure 4. Histogram of the values of z for the 10 day time interval.

distribution of waiting times (time elapsed between the end of a switchback and the onset of the next one) and of residence times (duration of a switchback) (Aschwanden et al. 2016). Numerous authors have investigated the waiting time distribution of intermittent events such as solar flares (e.g., Wheatland & Litvinenko 2002), radio bursts (e.g., Pulupa et al. 2020), and discontinuities in the solar wind (e.g., Greco et al. 2009). For a sequence of independent events that behave as a Poisson process; this distribution should be an exponential. In contrast, power-law distributions arise when events are correlated. In practice, the distinction between the can easily be blurred by additional effects. Non-stationarity associated with time-varying flaring rates, for example, causes the distribution to be exponential for short durations and to roll over to a power law for long durations (Lepreti et al. 2001; Wheatland & Litvinenko 2002).

Figure 5. Waiting time distribution of normalized deflection z for different thresholds.

Figure 6. Residence time distribution of normalized deflection z for different thresholds. The waiting time distributions from Figure 5 are shown in gray, for comparison.

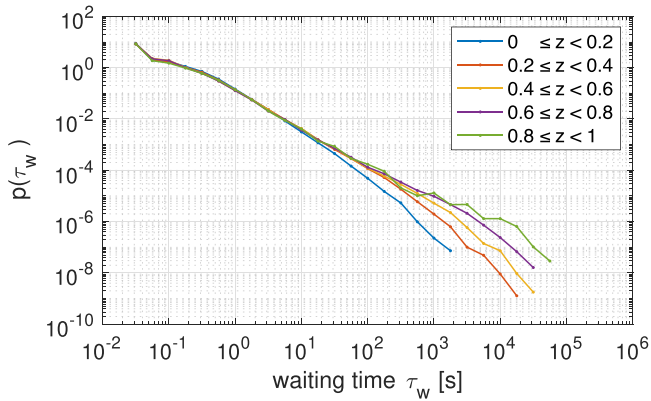Figure 5 summarizes the main results for the waiting time distribution using five thresholds of z. First, note how all the distributions collapse onto one single curve, except for the longest intervals that exceed hundreds of seconds. This is a strong indication that all deflections, whether small or large, have a common driver. Second, all distributions tend to follow a power law over several decades. The slope of this power law ranges between -1.4 and -1.6; similar values have been found in natural phenomena that exhibit clustering (Aschwanden et al. 2016). Note that the existence of such a power law implies that the mean waiting time is ill-defined.

Deviations from this power law for short waiting times can be explained by the presence of ion cyclotron waves (Bowen et al. 2020) and interference noise from the spacecraft that distort the distribution. Interestingly, the power law breaks down too at long timescales. Although finite sample effects become increasingly important there is also a systematic depletion of long waiting times associated with small deflections. This may be due to a dual waiting time distribution with a mix of clustered deflections that are responsible for a power law and occasional quiescent intervals that exhibit smaller deflections. If the latter were randomly distributed, then the tail of the waiting time distribution should roll over to an exponential distribution, with fewer events as compared to what a power law should give (Aschwanden et al. 2016).

Further insights can be gained from the residence time distribution. Surprisingly, the waiting and residence time distributions are (to a first approximation) remarkably similar; see Figure 6. This important result suggests that the same physical processes govern the onset and the termination of a deflection. One would expect this for entangled filaments (Parker 1963) or flux tubes (Borovsky 2008) that are moving past the spacecraft. If, on the other hand, the deflections were due to outward propagating perturbations that are generated in the lower corona then the underlying instability would more likely give rise to different distributions. The same would occur for a plasma oscillating between two metastable states.

Figure 6 also reveals a conspicuous excess of long-duration intervals with small deflections, which indicates that there is a tendency for the magnetic field to remain in the ground state that has small deflections. Conversely, there is a relative deficit of large deflections.

A new picture emerges: in the previous section we concluded that there was a continuum of deflections. Here, the waiting time distributions give a more contrasted picture in
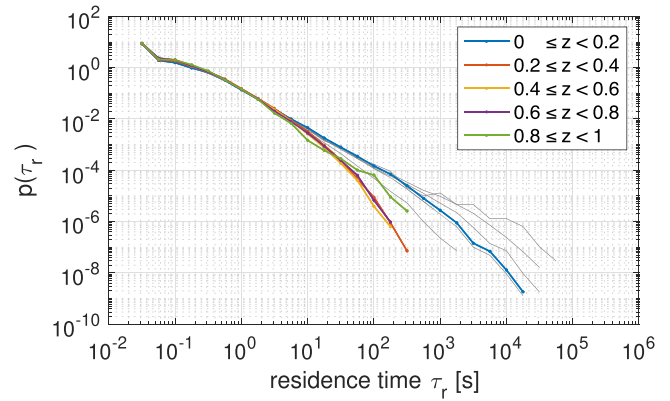
which the ground state is relatively more frequent, as if the magnetic field was staying by default in this ground state, and leaving it only during deflections. The omnipresence of the deflections gives the false impression that there is no distinction between them and the ground state.

To summarize, to a first approximation, the magnetic field behaves as a monostable system with a preferential ground state. Deflections away and back to this ground state are ruled by the same physical processes and their omnipresence leaves few opportunities for actually observing the ground state. The power-law scaling of the waiting time distribution suggests that deflections aggregate, whatever their magnitude. There are no noticeable differences in these scalings when one-day intervals are chosen.

5. Long Memory Effects

The clustering of consecutive deflections suggests that there is long memory in the coronal magnetic field. This memory may have several origins. The most obvious one is a temporal correlation associated with the spatial coupling between adjacent magnetic flux tubes, similar to what is observed in spin lattices. These flux tubes, when mapped back into the photosphere, correspond to granules or supergranules whose small motion at the solar surface gets amplified because of the expansion of the flux tubes, and naturally leads to temporal correlations. Disentangling these different causes without multipoint observations is challenging.

To find clearer evidence for clustering between switchbacks we correlate each waiting time to its consecutive values. Since the waiting times vary by orders of magnitude, it is more appropriate to correlate their ranks, similar to the difference between Pearson and Spearman rank correlation functions (Press et al. 2002). Here, by estimating the autocorrelation function of the ranked values, we quantify whether waiting times of a given rank are likely to be followed values of a similar rank for the next event, the second next event, and so on.

Figure 7 illustrates the results of the autocorrelation of ranked waiting times for a threshold of $z = 0.1$. Note the fast decay, which indicates that consecutive values rapidly differ from each other. The autocorrelation, however, does not drop to zero; its decay is well matched by a $C(\text{lag}) \propto \text{lag}^{-1/2}$ scaling that is indicative of long-range correlations (Beran 1994).
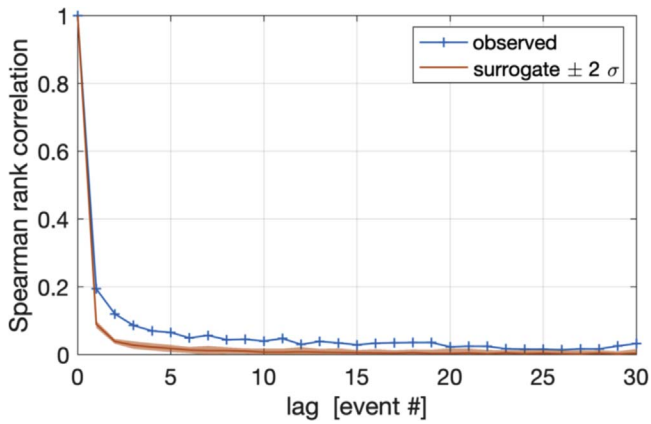
Figure 7. Autocorrelation of the sequence of ranked waiting times (determined with a threshold value of $z = 0.1$) for real observations and for surrogate data. For the latter, an average over 20 surrogates, with a $\pm 2\sigma$ interval are shown. Switchbacks that are shorter than 1 s have been excluded.

The significance of this long tail of the autocorrelation function requires careful evaluation. Instead of considering confidence intervals we use a more stringent test and use surrogate data (Schreiber & Schmitz 2000) to answer the question: do the nonzero correlations result from a nonlinear process that causes consecutive switchbacks to aggregate, or are they just a consequence of linear effects (i.e., the fact that nearby observations of the magnetic field are more likely to be similar)? More precisely, we test the null hypothesis that clustering in the normalized deflection z is produced by a Gaussian linear stochastic process. To do so, we generate surrogate time series of z that have the same probability distribution and same autocorrelation function (and therefore also the same power spectral density) as the initial record z. The characteristics of these surrogates are remarkably similar to those of the original data (a trained eye can barely distinguish them) and yet, whatever nonlinear correlation may exist in the magnetic field has been destroyed in the surrogates. From these we estimate the waiting times whose autocorrelation is then compared to that of the original values.

The comparison of the two autocorrelation functions in Figure 7 confirms the existence of a significant residual correlation between consecutive waiting times, which is absent in surrogate data. From this we conclude that there is a long memory in the sequence of switchbacks. Figure 7 in addition shows that this memory persists at least for a dozen consecutive deflections.

These conclusions remain valid with other thresholds although the results are more contrasted when the threshold is between 0.05 and 0.2. To better diagnose the origin of this long memory let us now consider Detrended Fluctuation Analysis (DFA; Beran 1994; Kantelhardt et al. 2001), which is particularly suited for detecting long memory in non-stationary time series.

In the following we consider zeroth order DFA or DFA0 (also known as fluctuation analysis Bryce & Sprague 2012) because we do not aim at removing trends. In DFA0 a sampled time series x_t is sliced into N_W non-overlapping windows of equal duration τ in each of which we calculate the variance. Finally, we consider the root mean variance

$$\sigma_x(\tau) = \sqrt{\frac{1}{N_W}\sum_{i=1}^{N_W}\langle(x_{t_i} - \langle x_t\rangle_{W_i})^2\rangle_{W_i}}, \quad (3)$$

in which $\langle\cdots\rangle_{W_i}$ stands for a time average over the interval $W_i : t_i \leqslant t \leqslant t_i + \tau$. For a self-affine process $\sigma(\tau) \propto \tau^\mu$, whose scaling exponent μ is related to the Hurst exponent. For uncorrelated fluctuations such as those resulting from Brownian motion, $\mu = \frac{1}{2}$, whereas for serial correlation one should have $\mu > \frac{1}{2}$. Conversely, $\mu < \frac{1}{2}$ implies anticorrelation. These scaling exponents embody a close correspondence with physical scenarios (Metzler et al. 2009).

Using DFA we can now compare the magnetic field with the normalized deflection, and also select intervals according to the magnitude of the deflections. This enables us to determine whether the evidence for long memory is the consequence of the switchbacks only or if it is intrinsic to the complete sequence of observations. In addition, by applying DFA to z and to the different components of the magnetic field, we should be able to determine whether the origin of long memory is geometrical and resides in the orientation of the magnetic field or if variations of the magnetic field amplitude contribute to it.

The results of DFA analysis are summarized in Figure 8. As before, we focus on the radial component of the magnetic field and consider two cases: quiescent conditions that should be close to the ground state ($z < 0.05$) and active conditions ($0 \leqslant z \leqslant 1$), both for z and for B_R.

The lower plot of Figure 8 displays the main quantity of interest, which is the scaling exponent μ. For quiescent conditions μ remains close to 0.5, except at short timescales ($\tau < 10\,s$), where coherent wave activity is likely to affect the results. Such a value of μ implies the absence of long memory in both B_R or z when the magnetic field is its ground state; it is also the signature of regular diffusion.

If, however, we apply DFA to active conditions, then the scaling exponent is systematically larger and saturates around 0.6. Such values are the signature of long memory, or at least longer lasting memory than in the quiescent regime. Numerous studies have shown how anisotropic magnetic fields such as those associated with meandering field lines can lead to anomalous superdiffusive particle transport (Jokipii & Parker 1969; Pommois et al. 2001; Perrone et al. 2013). In this context, the aggregation of the switchbacks also provides favorable conditions for non-diffusive transport.

Interestingly, the scaling exponents are nearly identical for z and for B_R; consequently, long memory effects occur in the angular deflections rather than in the fluctuations of the magnetic field that come on top of these. In other words, the long memory resides in the way switchbacks occur as events, while the background magnetic field fluctuations have limited memory.

The picture that emerges reveals a magnetic field whose ground state has no long memory, in contrast to the intermittent deflections that tend to aggregate and therefore exhibit long memory. These distinct properties corroborate the idea that the two have different origins. This surprising emergence of long memory in transient events rather than in the ground state has received considerable attention in the context of climate science because of its implications on predictability (Koutsoyiannis 2003). Franzke et al. (2015) have shown that it is precisely the rate of switching between different states (in our case, the occurrence of deflections) that can generate long memory and be responsible for non-stationarity in a system that is otherwise memoryless. Recently, Sato & Klages (2019) provided yet
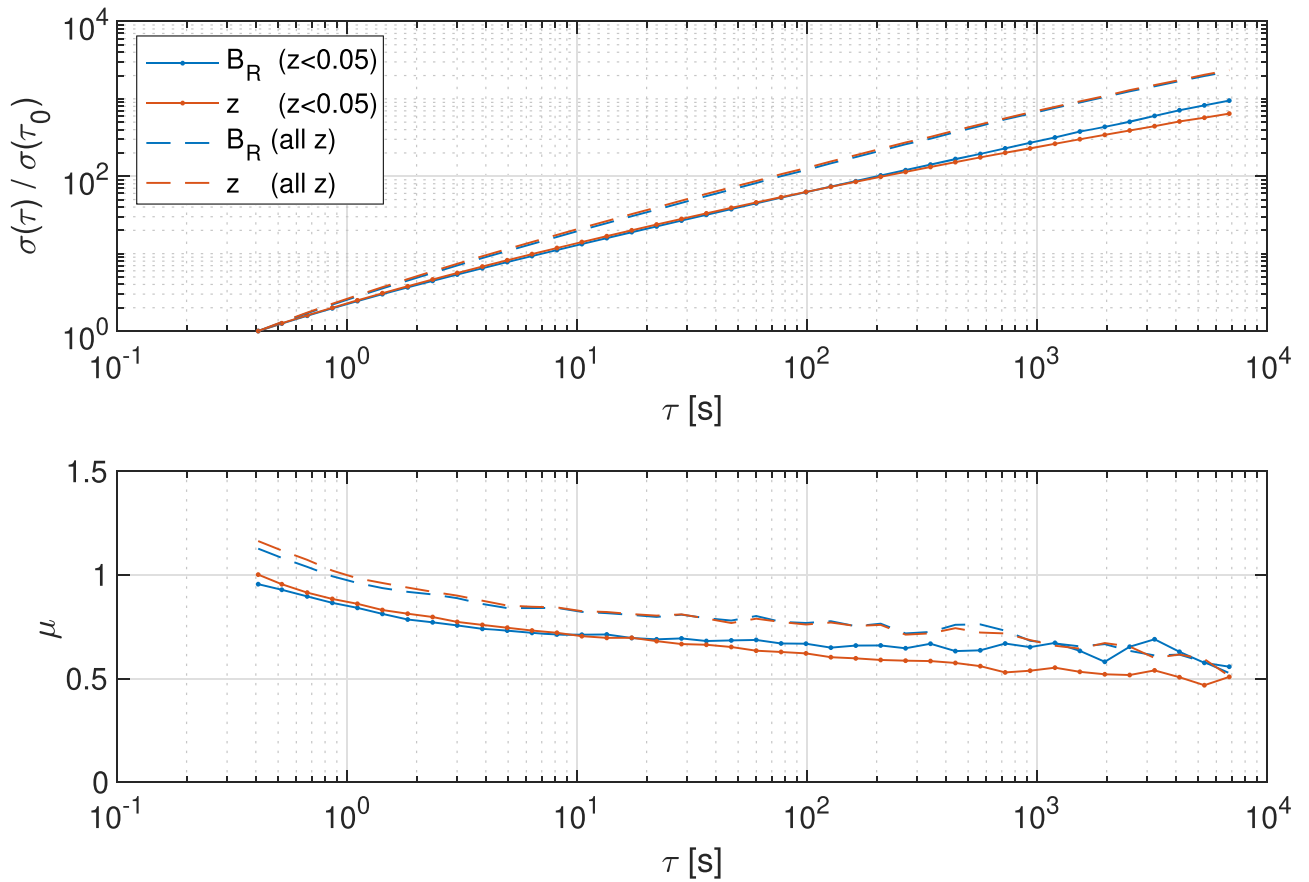
Figure 8. Detrended fluctuation analysis (DFA0) applied to B_R and to the normalized deflection z, for quiescent intervals and for active intervals. The upper plot shows $\sigma(\tau)$ normalized to its value for the shortest time; the lower plot shows the corresponding scaling exponent μ.

another explanation for this behavior by showing that particles that are sampled randomly either from a memoryless system with Brownian motion (i.e., our quiescent ground state) or from a non-chaotic system in which particles aggregate (i.e., switchbacks) exhibit anomalous diffusion with scaling exponents $\mu > 0.5$.

6. Impact on Turbulence Cascade

Now that there is evidence for the magnetic field fluctuations to have different origins depending on their deflection, let us turn to their spectral properties and determine whether switchbacks can be considered as being part of the turbulent wave field. For this, we consider the power spectral density of the different components of the magnetic field, and also of z, for specific thresholds on z. The results are summarized Figure 9 for quiescent conditions ($z < 0.05$) and active ones ($0 \leqslant z \leqslant 1$). The precise value of the threshold has no major impact on our conclusions as long as it properly isolates the quiescent state.

Since the quiescent state occurs only sporadically, we use the Lomb–Scargle method (Press et al. 2002; Vio et al. 2013) to estimate the power spectral density from irregularly sampled data and obtain access to timescales that exceed the duration of individual quiescent intervals. We systematically process in parallel a benchmark sequence with a known spectrum in order to check the validity of our results.

Figure 9 summarizes the main results by comparing the power spectral density of the radial component B_R for quiescent and for active conditions. In both regimes we observe power
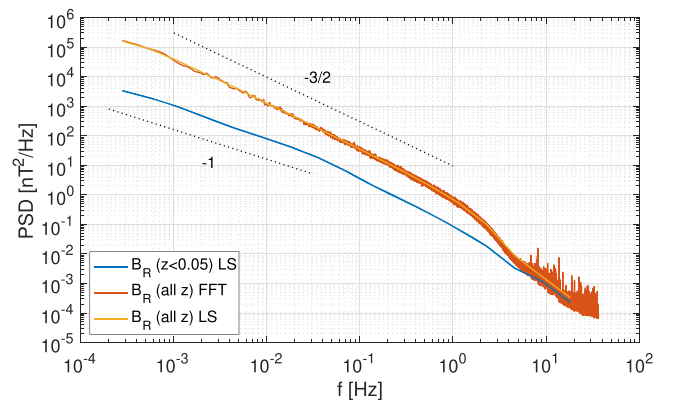

Figure 9. Power spectral density of the radial component B_R of the magnetic field for quiescent ($z < 0.05$) and active (all z) regimes. For the latter, we overplot the results obtained by using the Fast Fourier Transform (FFT) and the Lomb–Scargle (LS) method to confirm their good agreement.

laws $P(f) \propto f^\beta$ that extend over more than one decade. Frequencies above 1 Hz are discarded because they belong to the kinetic range. In addition, they are affected by narrowband noise from the spacecraft reaction wheels. The properties below 1 Hz in active conditions are typical for MHD turbulence, with an inertial range whose spectral index is close to $\beta = -3/2$, preceded by a so-called $1/f$ range whose slope is close to $\beta = -1$ (Chen et al. 2020). The break frequency between the two is located around 0.001 Hz, which is consistent with the fluctuation level of the magnetic field (Matteini et al. 2019).

Table 1
Spectral Index of the Power Spectral Density of B_R Estimated for Active
($0 \leqslant z \leqslant 1$) and Quiescent ($z < 0.05$) Conditions

Frequency Range [Hz]	Conditions	β
10^{-3}–$3 \cdot 10^{-2}$	Active	-1.50 ± 0.03
10^{-3}–$3 \cdot 10^{-2}$	Quiescent	-1.07 ± 0.03
$5 \cdot 10^{-2}$–1	Active	-1.63 ± 0.05
$5 \cdot 10^{-2}$–1	Quiescent	-1.70 ± 0.12

Figure 10. Same as Figure 9, but now comparing two components of the magnetic field and the total field for quiescent and active regimes. All estimates are based on the Lomb–Scargle (LS) method.

The active and quiescent regimes have comparable spectral indices between 0.05 and 1 Hz (which approximately correspond to the inertial range; see Table 1). At lower frequencies, however, the spectral index changes because the break frequency moves up from 0.001 to 0.05 Hz. The $1/f$ range is considered an energy reservoir of the turbulent cascade and consists of a mix of non-fully developed turbulence and coherent structures that still carry the signature of the sources of the wind (Bruno & Carbone 2013; Matteini et al. 2018). The fiftyfold increase in the break frequency may then suggest that in the quiescent regime the turbulent cascade has only had time to develop a short inertial range. In other words, the quiescent regime carries a signature of a more pristine and unevolved solar wind.

The same pattern arises in the power spectral density of the transverse components and the modulus of the magnetic field; see Figure 10, with some subtle differences that are beyond the scope of this study. Other effects may explain such a shift in the break frequency. Since the fluctuation level is lower in the quiescent regime, the turbulent eddies take longer to interact, which naturally shifts the break frequency upward. While this effect certainly plays a role, we note that by selecting larger thresholds of z (and thus allowing for eddies of larger amplitude) the break frequency does not immediately drop, as would be expected.

If quiescent conditions indeed correspond to a pristine solar wind, then how deep in the corona are these fluctuations generated? To answer this question we consider the correlation length of the magnetic field along the radial direction. The autocorrelation function of B_R decays monotonically and its e-folding time provides a coarse estimate of the decay time. By using a solar wind velocity model (Zouganelis et al. 2004) with the observed solar wind velocity as input, we can then approximately locate the source of the fluctuations. Let us stress that the decay time is indicative only because the magnetic field is non-stationary, so the autocorrelation function is biased (Jagarlamudi et al. 2019).

In the active regime the correlation time is of the order of a few minutes only because erratic deflections rapidly destroy the correlation. In the quiescent regime, however, the autocorrelation decays more slowly with a characteristic decay time of $T = 10 \pm 7$ (hr). The large uncertainty reflects the dispersion of the values as estimated from a sequence of 2 day intervals. Note that this decay time is biased and therefore should be considered a lower bound.

The long decay time associated with the quiescent regime corresponds to a source located below $20\,R_\odot$. This is lower than the Alfvén point, which is estimated to be located between 25 and $30\,R_\odot$ (Kasper et al. 2019). We conclude that the fluctuations that are seen during the quiescent regime c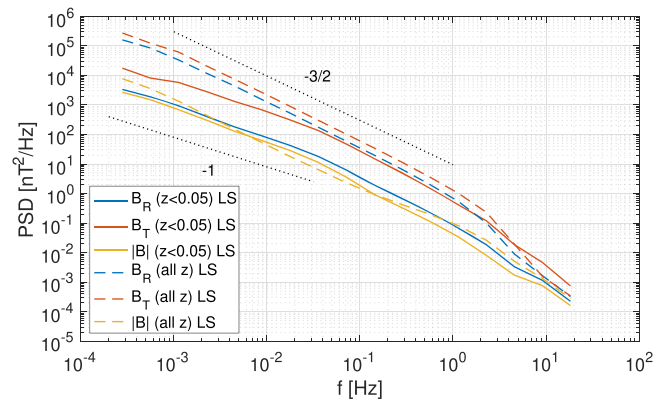orrespond to the transit of highly elongated structures that most likely originate deep inside the corona (possibly as deep as the photosphere).

7. Discussion and Conclusions

Our results lead to an apparent contradiction. On one hand we observe a continuum of deflections in the magnetic field, which suggests that there is only a single regime, with a seamless continuum between a quiescent state with small deflections, and large switchbacks. Here we ignore coherent wave activity that also occurs and is further addressed in Bowen et al. (2020) and Malaspina et al. (2020).

On the other hand, we find evidence for long memory in the deflections only and not in the quiescent regime. From this we conclude that the magnetic field is more likely to exhibit two regimes: a quiescent ground state with no long memory, and occasional perturbations (deflections) that do exhibit long memory.

The distinction between the two pictures brings us back to the initial question: are switchbacks part of the turbulent wave field or should they be considered as external perturbations? This distinction between the two, if it exists, is blurred by several effects, such as the small variations in the orientation of the Parker spiral.

Several indicators support the idea that switchbacks and the quiescent ground state are distinct. First, the similarity between the waiting and residence time distributions suggests that switchbacks correspond to a deviation from the ground state, which excludes the existence of a bistable state as observed, for example, in some plasma instabilities (Passot et al. 2006). Second, the relative excess of occurrences of long quiescent regimes is in favor of their different nature. A third indicator is the different spectral density of B_R, which we interpret as a signature of unevolved solar wind for the quiescent regime.

These indicators do not exclude alternate explanations such as one in which deflections would be remnants of large switchbacks that have evolved into fully developed turbulence. Here the turbulent wave field conserves imprints of the initial drivers. This may explain one of our puzzling results, which is the similarity of the spectral indices as inferred from the active regime and as reported for the inertial range of turbulence in the inner heliosphere (Chen et al. 2020) or in corresponding MHD turbulence models (Chandran et al. 2015), as if a mix of switchback with pristine unevolved solar wind equals inertial range turbulence. Note that this similarity could also be a mere

coincidence. Indeed, random transitions between states can easily give rise to power spectral densities that follow a power law with a spectral index located between -1 and -2. Incidentally, this highlights the ambiguity of the spectral index, for which completely different physical processes can give rise to comparable values.

If these switchbacks are distinct from the quiescent ground state, do the two eventually merge into a fully developed turbulence energy cascade? The study by Borovsky (2016) suggests that switchbacks do not evolve after 0.3 AU, as if they had stopped interacting with the surrounding turbulent wave field. Several studies suggest that switchbacks observed closer to the Sun by *Parker Solar Probe* do interact with the ambient magnetic field: Krasnoselskikh et al. (2020) argue that wave activity at the boundary of switchbacks may contribute to mixing and eventually to their weakening, while Tenerani et al. (2020), using simulations, conjecture that they originate in the lower corona and survive out to *Parker Solar Probe* distances. All these results support the idea that the concentration of switchbacks is higher at the perihelion of *Parker Solar Probe* than farther out. Note, however, that our perception is biased by the near-corotation of the spacecraft with the Sun, which favors the observation of radial structures advected over the spacecraft rather than the crossing of magnetic flux tubes.

At this stage we are unable to nail down the precise origin of these switchbacks, for which a microscopic investigation of the wave and particle properties is required. However, our macroscopic analysis favors mechanisms in which these structures can be described as temporary departures from a ground state with a strong spatial correlation in the source of these deflections. Both switchbacks and the quiescent solar wind must originate deep in the corona. This picture is more difficult to reconcile with jets that would be produced by reconnection events lower in the corona because the rate of occurrence of the latter is unlikely to exhibit long memory. For the same reason, it is more difficult to reconcile with a model that would involve self-organized criticality. On the contrary, the picture is compatible with the meandering of kinked magnetic field lines.

To conclude, let us summarize the main facts, and then proceed with more speculative results.

1. First, we find that magnetic switchbacks come in all durations (seconds to hours) and all angular deflections (0°–180°) with respect to the Parker spiral. They are best observed in radial component of the magnetic field, on which this study focuses. The bulk of the distribution (more than 98%) is isotropically distributed around the Parker spiral and can therefore be conveniently described by one single dimensionless quantity, which we call the normalized deflection. From the distribution of deflections we conclude that there is no crisp definition of what a switchback is. Rather, we are in the presence of a continuum of deflections that could typically result from a fractal distribution of kinked magnetic flux tubes.

2. Both the waiting time and residence time distribution of these deflections tend to follow a power law and are remarkably similar. This suggests that consecutive deflections tend to aggregate. Furthermore, the onset and termination of a deflection must be governed by the same physical processes. Finally, the magnetic field does not behave as a system with different metastable states, but rather as a monostable system that moves away from its ground state for each deflection. This explains the relative excess of long quiescent time intervals (i.e., with small deflections of typically $z < 0.1$).

3. Autocorrelation and DFA confirm the presence of long memory in the magnetic field. Interestingly, this long memory manifests itself in the occurrence of deflections and not in the fluctuations that are observed during the quiescent regime. Such anisotropies of the magnetic field with long-range correlations offer are known to generate anomalous particle transport (Pommois et al. 2001).

   Recently, Sato & Klages (2019) showed how similar behavior arises in systems that result from a mix between memoryless Brownian motion and non-chaotic aggregation. The long memory we observe is most likely associated with the strong spatial connection between adjacent magnetic flux tubes and their common photospheric footpoints (e.g., Borovsky 2008).

4. While the power spectral density of the magnetic field data is consistent with scaling laws found for the inner heliosphere (Chen et al. 2019; Matteini et al. 2019) the quiescent regime exhibits a longer $1/f$ range. We conjecture that this quiescent regime corresponds to a more pristine solar wind whose spectral energy cascade has only had time to develop a short inertial range. From its correlation length we estimate its source to be located below $20\,R_\odot$, i.e., well below the Alfvén point.

   Surprisingly, the spectral properties of the mix between switchback and quiescent solar wind equals that of classical solar wind turbulence, which raises questions as to how much these switchbacks actually interact and merge with the background turbulence.

Taken together, these results suggest that switchbacks are probably not inherently part of the turbulent wave field but are remnants of strong deflections that occurred deeper down in the corona and are connected by their common origin. Their spectral signature mimics that of inertial range turbulence, which suggest that they are gradually merging with it. In contrast, the spectral signature of the quiescent magnetic field between switchbacks is reminiscent of a more pristine and less evolved solar wind. These properties, and in particular the long memory of the rate of occurrence of switchbacks, are compatible with a physical picture in which these structures are the signature of kinked magnetic flux tubes that are moving past the spacecraft. The combined long memory and high anisotropy of these events offer favorable conditions for anomalous particle transport.

Facility: Parker Solar Probe.

ORCID iDs

Thierry Dudok de Wit ⓘ https://orcid.org/0000-0002-4401-0943
Vladimir V. Krasnoselskikh ⓘ https://orcid.org/0000-0002-6809-6219
Stuart D. Bale ⓘ https://orcid.org/0000-0002-1989-3596
John W. Bonnell ⓘ https://orcid.org/0000-0002-0675-7907
Trevor A. Bowen ⓘ https://orcid.org/0000-0002-4625-3332
Christopher H. K. Chen ⓘ https://orcid.org/0000-0003-4529-3620
Clara Froment ⓘ https://orcid.org/0000-0001-5315-2890
Keith Goetz ⓘ https://orcid.org/0000-0003-0420-3633
Peter R. Harvey ⓘ https://orcid.org/0000-0002-6938-0166
Vamsee Krishna Jagarlamudi ⓘ https://orcid.org/0000-0001-6287-6479
Andrea Larosa ⓘ https://orcid.org/0000-0002-7653-9147
Robert J. MacDowall ⓘ https://orcid.org/0000-0003-3112-4201
David M. Malaspina ⓘ https://orcid.org/0000-0003-1191-1558
William H. Matthaeus ⓘ https://orcid.org/0000-0001-7224-6024
Marc Pulupa ⓘ https://orcid.org/0000-0002-1573-7457
Marco Velli ⓘ https://orcid.org/0000-0002-2381-3106
Phyllis L. Whittlesey ⓘ https://orcid.org/0000-0002-7287-5098

References

Araujo, F. F., Grossmann, S., & Lohse, D. 2005, PhRvL, 95, 084502
Aschwanden, M., Crosby, N., Dimitropoulou, M., et al. 2016, SSRv, 198, 47
Badman, S. T., Bale, S. D., Martínez Oliveros, J. C., et al. 2020, ApJS, doi:10.3847/1538-4365/ab4da7
Bale, S. D., Goetz, K., Harvey, P. R., et al. 2016, SSRv, 204, 49
Bale, S. D., Badman, S. T., Bonnell, J. W., et al. 2019, Natur, 576, 237
Balogh, A., Forsyth, R. J., Lucek, E. A., Horbury, T. S., & Smith, E. J. 1999, GeoRL, 26, 631
Behannon, K. W., & Burlaga, L. F. 1981, in Solar Wind 4, ed. H. Rosenbauer (Garching: Max-Planck-Institute für Aeronomie), 374
Belcher, J. W., & Davis, L., Jr. 1971, JGR, 76, 3534
Benzi, R. 2005, PhRvL, 95, 024502
Beran, J. 1994, Statistics for Long-memory Processes (New York: Chapman and Hall)
Borovsky, J. E. 2008, JGRA, 113, 8110
Borovsky, J. E. 2016, JGRA, 121, 5055
Bowen, T., Mallet, A., Klein, K. R., et al. 2020, ApJS, doi:10.3847/1538-4365/ab6c65
Bruno, R., & Carbone, V. 2013, LRSP, 2, 4
Bryce, R. M., & Sprague, K. B. 2012, NatSR, 2, 315
Chandran, B. D. G., Schekochihin, A. A., & Mallet, A. 2015, ApJ, 807, 39
Chen, C. H. K., Bale, S. D., Bonnell, J. W., et al. 2020, ApJS, doi:10.3847/1538-4365/ab60a3
Farge, M., & Schneider, K. 2015, JPlPh, 81, 435810602
Fox, N. J., Velli, M. C., Bale, S. D., et al. 2015, SSRv, 204, 7
Franzke, C. L. E., Osprey, S. M., Davini, P., & Watkins, N. W. 2015, NatSR, 5, 9068
Gammaitoni, L., Hänggi, P., Jung, P., & Marchesoni, F. 1998, RvMP, 70, 223
Gosling, J. T., McComas, D. J., Roberts, D. A., & Skoug, R. M. 2009, ApJL, 695, L213

Greco, A., Matthaeus, W. H., Servidio, S., & Dmitruk, P. 2009, PhRvE, 80, 046401
Horbury, T. S., Woolley, T., Laker, R., et al. 2020, ApJS, doi:10.3847/1538-4365/ab5b15
Horbury, T. S., Matteini, L., & Stansby, D. 2018, MNRAS, 478, 1980
Howard, R., Vourlidas, A., Bothmer, B., et al. 2019, Natur, 576, 232
Jagarlamudi, V. K., Dudok de Wit, T., Krasnoselskikh, V., & Maksimovic, M. 2019, ApJ, 871, 68
Jokipii, J. R., & Parker, E. N. 1969, ApJ, 155, 777
Kahler, S. W., Crooker, N. U., & Gosling, J. T. 1996, JGR, 101, 24373
Kantelhardt, J. W., Koscielny-Bunde, E., Rego, H. H. A., Havlin, S., & Bunde, A. 2001, PhyA, 295, 441
Kasper, J. C., Bale, S. D., Belcher, J. W., et al. 2019, Natur, 576, 228
Koutsoyiannis, D. 2003, Hydrological Sci. J., 48, 3
Krasnoselskikh, V. V., Larosa, A., Agapitov, O., et al. 2020, ApJS, submitted
Landi, S., Hellinger, P., & Velli, M. 2006, GeoRL, 33, L14101
Lepreti, F., Carbone, V., & Veltri, P. 2001, ApJL, 555, L133
Malaspina, D. M., Halekas, J., Bale, S. D., et al. 2020, ApJS, doi:10.3847/1538-4365/ab4c3b
Matteini, L., Horbury, T. S., Neugebauer, M., & Goldstein, B. E. 2014, GeoRL, 41, 259
Matteini, L., Stansby, D., Horbury, T. S., & Chen, C. H. K. 2018, ApJL, 869, L32
Matteini, L., Stansby, D., Horbury, T. S., & Chen, C. H. K. 2019, NCimC, 42, 16
McComas, D., Christian, E., Cohen, C., et al. 2019, Natur, 576, 223
McManus, M. D., Bowen, T. A., Mallet, A., et al. 2020, ApJS, doi:10.3847/1538-4365/ab6dce
Metzler, R., Chechkin, A. V., & Klafter, J. 2009, in Encyclopedia of Complexity and System Science, ed. R. A. Meyers (New York: Springer), 1724
Neugebauer, M. 2012, ApJ, 750, 50
Neugebauer, M., & Goldstein, B. E. 2013, in AIP Conf. Proc. 1539, SOLAR WIND 13, ed. G. P. Zank et al. (Melville, NY: AIP), 46
Nicolis, C. 1993, JSP, 70, 3
Parker, E. N. 1963, Interplanetary Dynamical Processes (New York: Interscience Publishers)
Passot, T., Ruban, V., & Sulem, P. L. 2006, PhPl, 13, 102310
Peierls, R. 1936, PCPS, 32, 477
Perrone, D., Dendy, R. O., Furno, I., et al. 2013, SSRv, 178, 233
Pommois, P., Veltri, P., & Zimbardo, G. 2001, JGR, 106, 24965
Press, W. H., Teukolsky, S. A., Vetterling, W. T., & Flannery, B. P. 2002, Numerical Recipes: the Art of Scientific Computing (3rd ed.; Cambridge: Cambridge Univ. Press)
Pulupa, M., Bale, S. D., Badman, S. T., et al. 2020, ApJS, doi:10.3847/1538-4365/ab5dc0
Sato, Y., & Klages, R. 2019, PhRvL, 122, 174101
Schreiber, T., & Schmitz, A. 2000, Physica D, 142, 346
Sorriso-Valvo, L., Stefani, F., Carbone, V., et al. 2007, PEPI, 164, 197
Tenerani, A., Velli, M., Matteini, L., et al. 2020, ApJS, doi:10.3847/1538-4365/ab53e1
van Ballegooijen, A. A., Cartledge, N. P., & Priest, E. R. 1998, ApJ, 501, 866
Velli, M., Lionello, R., Linker, J. A., & Mikić, Z. 2011, ApJ, 736, 32
Vio, R., Diaz-Trigo, M., & Andreani, P. 2013, A&C, 1, 5
Wheatland, M. S., & Litvinenko, Y. E. 2002, SoPh, 211, 255
Whittlesey, P., Kasper, J. T., Bale, S. D., et al. 2019, ApJS, submitted
Yamauchi, Y., Suess, S. T., Steinberg, J. T., & Sakurai, T. 2004, JGRA, 109, A03104
Zouganelis, I., Maksimovic, M., Meyer-Vernet, N., Lamy, H., & Issautier, K. 2004, ApJ, 606, 542